PROCEEDINGS OF THE SIXTEENTH LUNAR AND PLANETARY SCIENCE CONFERENCE, PART 2
JOURNAL OF GEOPHYSICAL RESEARCH, VOL. 91, NO. B4, PAGES D413–D430, MARCH 30, 1986

Impact Craters of Venus: Analysis of Venera 15 and 16 Data

B. A. IVANOV

O. Yu. Schmidt Institute of the Earth Physics, USSR Academy of Science, Moscow

A. T. BASILEVSKY, V. P. KRYUCHKOV, I. M. CHERNAYA

V. I. Vernadsky Institute of Geochemistry and Analytical Chemistry, USSR Academy of Science, Moscow

From description of impact craters on Venus and crater size-and-depth distributions, models are developed that analyze the size-distribution curve and radar-bright haloes around fresh craters. The dense Venusian atmosphere has a strong influence on cratering. The estimated age of the surface of the area under study is from 0.5 to 1.0 $\times 10^9$ years. The estimated rate of resurfacing during this time interval is about 0.04 to 0.8 cm/10^6 years. The lithosphere of Venus seems to be sufficiently rigid to sustain craters of 100–140 km diameter and 0.8–2.5 km depth for about 10^8 years.

1. INTRODUCTION

The existence of impact craters on Venus has been suspected for some time. Calculations have shown that the Venusian atmosphere could not effectively decelerate relatively large meteoroids [see, for example, *Petrov and Stulov*, 1975]. Large circular features of probable impact origin were revealed by Pioneer Venus and earth-based radar pictures [see, for example, *Masursky et al.*, 1980; *Campbell and Burns*, 1980], but the low resolution of the images did not provide convincing evidence for an impact origin for these features. In contrast, the images of the Venusian surface obtained by the side-looking radars of Venera 15 and 16 have a much higher resolution (1 to 2 km), including large areas of stereo-overlap that allow reliable identification of craters and morphologic evidence for their impact origin. A description of the imaging technique as well as the general characteristics of the geologic setting of the surveyed area is given in a companion paper [*Barsukov et al.*, 1985].

2. CONSIDERATION OF THE OBSERVATIONAL DATA

2.1. General Morphology

The radar images of Veneras 15 and 16 display craters whose morphology is similar to that of the impact craters of the Moon, Mercury, Mars, and other planetary bodies [e.g., *Basilevsky et al.*, 1983] (Figures 1–3). Craters with a diameter as small as of about 10 km, in some cases 4–5 km, are reliably identified. The largest craters so far identified are 100 to 140 km in diameter. The craters are superimposed upon various photogeologic units, including plains, highland volcanic plateaus, and ridge-and-groove mountains.

Most of the craters are circular depressions with elevated rims and central peaks (Figure 1). The freshest craters have radar-bright haloes that extend as much as 1 to 2 crater diameters. Commonly, the haloes display bilateral symmetry (Figure 4*a–d*), indicative of oblique impact [*Gault and Wedekind*, 1978] (Figures 2–4). The central peak craters of Venus, which are morphologically similar to the lunar craters of the Romer, Tycho, and Copernicus types [*Florensky et al.*, 1976], are typically in the diameter range of 10 km (limit of reliable "geologic" resolution) to 50–60 km.

Some craters have a bowl-shaped morphology (Figure 5). They are less abundant than those with central peaks. Those that are fresh also display elevated ring-like rims and radar-bright haloes. The sizes of well-preserved bowl-shaped craters range from 4–27 km. A few concentric ring craters similar to the well-known multiringed basins of the moon, Mercury, and Mars have been observed. The largest and morphologically most prominent is the circular depression of 140 km diameters north of Tethus Regio (Figure 6). Its outer and inner rings (140 and 105 km, respectively) are comprised of noncontinuous ridges, 10–20 km wide. The interring trough has a flat and, in places, knobby floor. The terrain inside the inner ring is knobby at the periphery and is smoother near the center. At the center there is a hill of about 15 km diameter. The basin is surrounded by a ring-like zone of smooth terrain 40–60 km wide, which is superimposed on the ridge-and-band pattern of the target plain. This is probably the ejecta blanket.

Other examples of double-ring basins on Venus include several craters 30–70 km in diameter, and two craters 100 km in diameter. Among the latter is Cleopatra Patera, a 100-km crater on the eastern slope of Maxwell Montes (Figure 7). Its inner ring is about 50 km in diameter. Its outer rim has a subdued appearance and is only slightly higher than the adjacent terrain. The inner ring is offset westward with respect to the outer ring and forms a prominent ridge in the east, but is more subtle in the west. Around the Cleopatra Patera is a zone of smooth terrain indicative of mantling of the adjacent ridge-and-groove terrain. The impact origin of Cleopatra Patera is under debate. Its double-ring structure is typical of large impact basins but the tectonic ridges around it show some elliptical orientation with the crater in the center consistent with an endogenic origin.

2.2. Morphological Classes

Topographically, Venusian craters range from fresh features with sharp rim crests and clear radar-bright haloes to highly degraded and smooth structures. We have distinguished four morphologic classes (Figure 8): (I) Fresh craters with prominent outlines and details of inner structure and well-developed radar-bright haloes. (II) Craters that have lost the prominent radar-bright halo but have clearly preserved the details of the inner structure. (III) Craters with the subdued details in the inner

Paper number 5B7003.
0148-0227/86/005B-7003$05.00

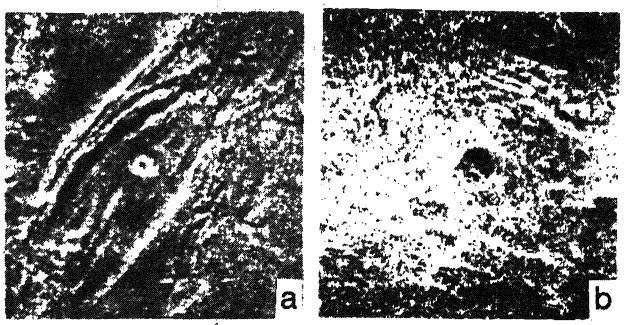

Fig. 1. Central-peak craters (*a*) 25 km and (*b*) 30 km in diameter.

structure and no ejecta zone. (IV) Highly degraded craters with very subdued morphology; in some cases impact origin may even be questionable. Most craters belong to classes I and II (nearly 25% and 40%, respectively). Craters belonging to classes III and IV are less abundant (near 25% and 10%, respectively). The relationship between morphological maturity and size is given in Table 1.

With increasing diameter, the frequency of the freshest craters (class I) tends to decrease; the frequency of slightly degraded craters (class II) varies, and the frequency of degraded and highly degraded craters (classes III and IV) increases with larger structures.

Some circular features of an unclear nature were revealed on the images [*Barsukov et al.*, 1985]. At least some of them may be severely modified impact craters. The description and analysis of these features will be given elsewhere (Nikolaeva et al., unpublished data, 1985). They are not considered further in this paper, nor are craters of obvious volcanic or tectonic-collapse origin [see *Barsukov et al.*, 1985].

2.3. Density of Craters

The crater density was determined for an area of 85×10^6 km^2. A total of 139 craters having diameters from 8 to 130 km have been counted. Their size distribution is given in Table 2. Plotting these data in an incremental manner (Figure 9), the distribution of impact craters of Venus appear unimodal. Over the observed range the distribution is lognormal in contrast to the exponential distribution of impact craters of the same size on the moon, Mercury, and Mars. This difference is evidently a result of the cut-off effect on crater-forming projectiles by the dense Venusian atmosphere. This phenomenon must be taken into account in any attempt to estimate ages of Venusian surfaces using crater densities (see below). The observed deficit of small craters, however, can also in part be related to the resolution limit of the Venera images and to the geometry of the radar illumination.

2.4. Radar-bright Haloes

An interesting and partly unexpected characterisitic of impact craters on Venus is the presence of prominent radar-bright haloes surrounding fresh craters. As mentioned above, many haloes display a clear bilateral symmetry (Figure 10). The maximum radial extent of the radar-bright haloes (L_m) as a function of crater diameter (D^r) are given in Table 3.

The high radar brightness of the halo is evidently a result of its greater surface roughness, on a scale equal to or greater than the sounding radio-wave length (8 cm). Such roughness can be formed by ejecta fragments, by secondary crater pits, or by other impact-induced disturbances of the surface. An analysis of this phenomenon demands considerations of ballistic transport through the dense atmosphere and the possible effects of shock air-waves accompanying the impact.

2.5. Depth of Craters

The Venera 15 and 16 spaceprobes had two separate radar systems: one for imaging, another for altimetry. The altimetry radar signal had a surface spot of 50 km in diameter and about 50 m resolution in elevation (in the case of smooth surfaces). In the case of rough surface, the altimetry signal is a weighted average for the entire radar footprint. The known curve of weight function (the relative contribution of different parts of the radar footprint), and superposition of adjacent altimetry measurements permits in principle improving the resolution of the altimeter substantially over that of an initial footprint. This work is now in progress. In this paper we use the original, unprocessed data of the altimetry radar. Because of the higher level of signal of the central part of radar spot relative to its periphery, the radar profile gives smoothened but visible relief along the spaceprobe trajectory, even for features less than 50 km in width.

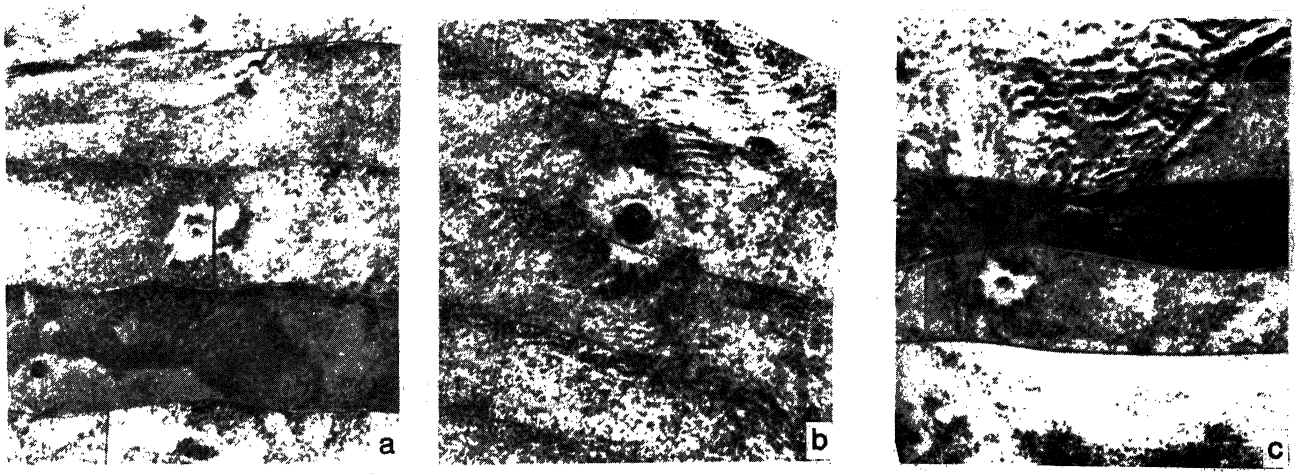

Fig. 2. Several examples of craters having an asymmetric radar-bright halo with the radar-dark outer halo. The craters are (*a*) 30 km, (*b*) 35 km, and (*c*) 15 km in diameter.

Fig. 3. Morphologically fresh central-peak crater (D ≃ 60 km) with a prominent halo of bilateral symmetry and a double-ringed basin (D ≃ 100 km) with higher morphological maturity.

In several cases the trace of the altimetry beam crossed an impact crater (Figure 11). The depth estimates were derived by connecting the rim points of the profile with a straight line and measuring the maximum depth from this line (Figure 11*a*). The approximate positions of the altimeter traces relative to crater rims are shown on Figure 11 also. The uncertainty of these positions and smoothening of profiles prevent the quantification of error estimates (Table 4), but most errors will lead to underestimates of the depths. Therefore the data in Table 4 should be considered as a lower limit of the real values.

3. MODELS

This section is a brief review of the models that will be used in further discussions of cratering on Venus.

3.1. The Atmosphere of Venus

The composition, temperature, pressure, and density of the atmosphere of Venus are now well known. The typical model of atmosphere by *Moroz* [1981], which is in excellent agreement with the direct measurements of the landed probes, may be analytically approximated as an isentrope of carbon dioxide, CO_2, with $\gamma = 1.2$ and surface ($z = 0$) parameters: temperature ($T = 735$ K), pressure ($p = 90$ atm), and density ($\rho^\circ = 64.8$ kg m^{-3}). The density decreases with height z as

$$\rho_a = \rho_o(1 - z/H)^5 \quad (1)$$

where the atmospheric maximum height H is

$$H = 94.8 \text{ km} \quad (2)$$

For heights of about H and higher, the real atmosphere does not obey (1).

Equation (1) is different from the usual exponential form of the Earth's atmosphere, because it is developed with an isothermal rather than an adiabatic model. Two simple illustrations clearly show the awesome properties of the Venusian atmosphere. If the whole atmosphere were condensed into a layer of near-surface constant density 64.8 kg m^{-3}, the thickness of this layer would be equal to

$$H_o = 15.4 \text{ km} \quad (3)$$

Fig. 4. Elliptical crater 45 × 55 km with asymmetric radar-bright halo. The maximum distance of the halo outer boundary from the crater center is as large as 120 km. This crater may have formed by oblique impact.

The mass of Venusian atmosphere is equivalent to a rock layer with a density of 3000 kg m^{-3} and thickness

$$H_{eq} = 330 \text{ m} \quad (4)$$

3.2. *Meteoroid Passage Through the Venusian Atmosphere*

The most probable entry velocity of meteoroids on Venus is in the range of 18–25 km s^{-1} [*Hartmann*, 1977]. The maximum pressures on the front surface of a body, $p_a = \rho_a v^2$, as a function of altitude, moving through the Venusian atmosphere with velocity v = 20 km/s are shown on Figure 12. Although there are considerable uncertainties in the mechanical properties of potential impactors, one may suppose that their cohesive strength does no exceed 0.01–0.1 GPa. Such stresses would be exceeded at altitudes of 0.7–0.8 H ≃ 60–80 km above the surface of Venus (A and B on Figure 12). Let us assume that projectiles at the time of impact behave as Coulomb-Mizes materials with a coefficient of internal friction of 0.3–0.5 [*Knowles and Brode*, 1977]. The limit of shear strength of such materials under ambient pressures larger than 4–5 GPa does not exceed 1–2 GPa [see, for example, *Trulio*, 1977; *Ullrich et al.*, 1977]. Such pressures on the front lobe of the entering body would occur at altitudes of 0.3 H ≃ 30 km (C on Figure 12).

The characteristic dimension of a body strongly decelerated by the atmosphere is about

$$L_e \simeq H_{eq} = 330 \text{ m} \quad (5)$$

because of momentum conservation. One may conclude that the failure condition may be reached with a rather small decrease of the meteoroid velocity for body diameters >>1 km, because of the high value of the dynamic pressure at the stagnation point. Thermal ablation would play a minor role for such bodies in comparison with inertial forces, which tend to destroy or deform high-velocity meteoroids in the atmosphere of Venus [*Grigoryan*, 1979].

We may conclude that at altitudes of about 70–80 km the high-velocity meteoroid starts to deform inelastically and that the deformation approaches hydrodynamic conditions at altitudes z ≃ 30 km.

A qualitative model of meteoroid deformation during atmosphere entry was developed by *Grigoryan* [1979]. He demonstrated that a good first approximation of this process is the flow of incompressible meteoroid material due to dynamic pressure on the front surface. *Grigoryan* [1979] treats the internal motion of meteoroid material with the usual equations of motion

$$\frac{\partial \vec{u}}{\partial t} + (\vec{u} \cdot \vec{\nabla}) \cdot \vec{u} = - \frac{\partial \sigma_{ij}}{\partial x_j} \quad (6)$$

where $\vec{u}$ is the relative velocity of internal flow of meteoroid material and σ_{ij} is the stress tensor. He distinguishes two stages of deformation: (1) a nonsteady, transitional stage, when

$$\left| \frac{\partial \vec{u}}{\partial t} \right| \gg \left| (\vec{u} \cdot \vec{\nabla}) \cdot \vec{u} \right| \quad (7a)$$

and (2) a quasistationary stage, when

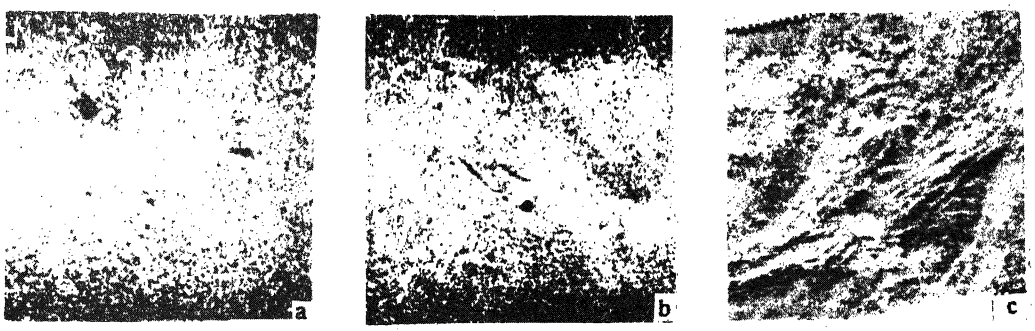

Fig. 5. Bowl-shaped craters: group of craters (*a*) 4–8 km in diameter in the Lakshmi Planum at the base of the Akna Montes crater, (*b*) 10 km, and (*c*) 25 km in diameter.

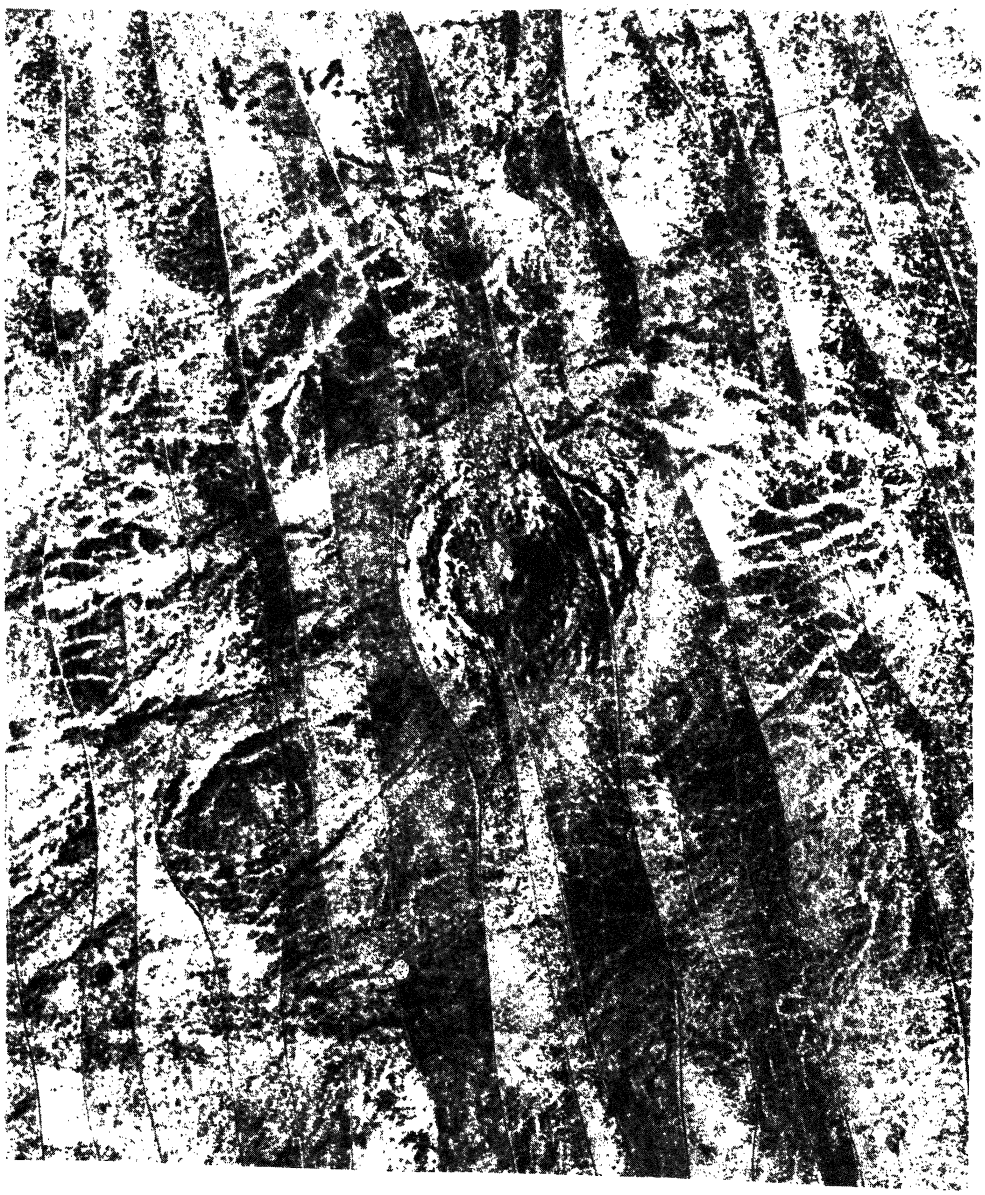

Fig. 6. Double-ring impact basin of about 140 km in diameter. Ejecta are superimposed on the ridge-and-band plain.

$$\left| \frac{\partial \vec{u}}{\partial t} \right| \ll \left| (\vec{u} \cdot \vec{\nabla}) \cdot \vec{u} \right| \tag{7b}$$

We have evaluated the deceleration and deformation of a liquid cylindrical body entering the Venusian atmosphere at high velocity, using the Grigoryan method. The initial diameter of the body L_o is assumed to be equal to its length l_o. This body was then assumed to flow under an aerodynamic pressure of a cylinder decreasing in length and increasing in diameter.

In this approximation one may derive the universal equation of motion in terms of the scaled coordinate w

$$w = \lambda^{1/7} \cdot (1 - z/H) \tag{8}$$

where

$$\lambda = \frac{\rho_o}{\rho_p} \left(\frac{H^2}{L_o \cdot \sin\alpha} \right)$$

ρ_p is the projectile density, L_o the initial projectile diameter, and α is the entry angle relative to the horizontal. ρ_o and H are described in (1).

For $\rho_p = 3000$ kg m^{-3}

$$\lambda^{1/7} = \frac{2.12}{(L_o \cdot \sin\alpha)^{2/7}} \tag{9}$$

Thus a projectile with $L_o \sin\alpha = 1$ km passing through the atmosphere to the surface $z = 0$ is equal to an increase in w from zero to 2.12.

The flattening of the body may be expressed in terms of its relative thickness as a function of w

$$l/l_0 = f(w) \tag{10}$$

This function, given by numerical calculation in our model,

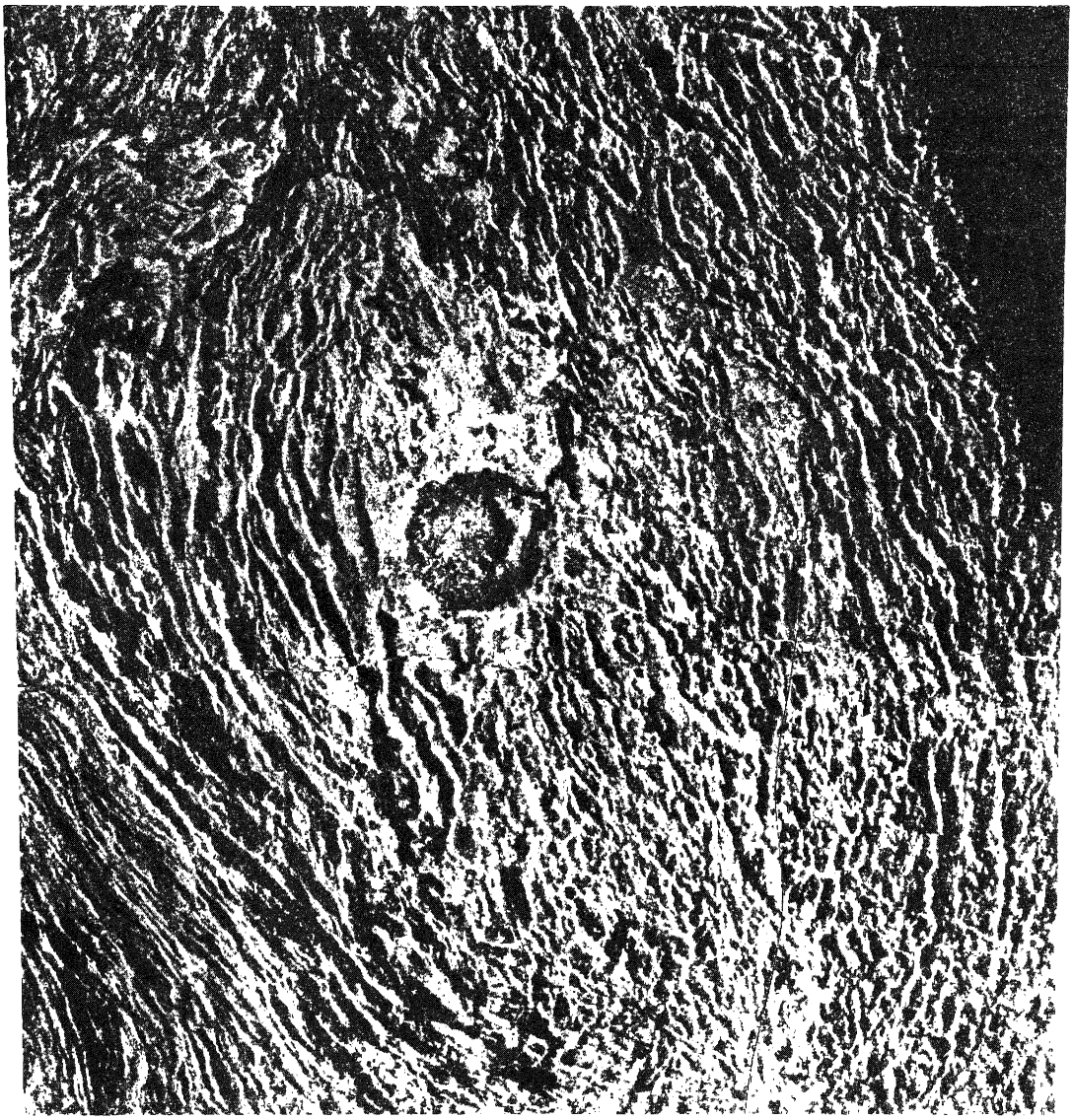

Fig. 7. Cleopatra Patera, about 100 km in diameter.

is shown in Figure 13. The diameter of a body increases as $L/L_o = \sqrt{l/l_o}$. The Grigoryan model supposes that the flattening body would tend to become an aerodynamically stable form with a blunt nose. On the basis of experiments with high-speed metal projectiles [*Beliakov et al.*, 1964] and with upstream, supersonic gas jets [e.g., *Romeo and Sterrett*, 1965], one may conclude that the radius of curvature of such a blunt-nosed body would be approximately twice its initial diameter. For $L/L_o \lesssim 2$, fragments of the periphery of the body would be detached from the main body because of hydrodynamic instability, and would further decelerate in the ambient gas. Thus after $L/L_o \lesssim 2$, a substantial decrease of the mass of the body may occur.

The dashed line on Figure 13 corresponds to the case (6*a*), which describes the decreasing thickness of a very porous body. The decrease of the velocity of a deforming body in our model may be expressed as

$$V/V_o = \exp\left[\sqrt{\rho_o/\rho_o} \cdot \lambda^{-3/14} \cdot J(w)\right] \qquad (11)$$

where the function

$$J(w) = \int_o^w l_0/l \cdot w^5 \cdot dw$$

is shown on Figure 13. Equations (10) and (11) give only the limit for a weak body and calculations for finite-strength bodies moving through a dense atmosphere need to be performed. Conversion of crater diameters into projectiles of specific initial dimensions has been done on the basis of (1) impact-explosion analogy [*Oberbeck*, 1971; *Bryan et al.*, 1980] and (2) scaling relationships [*Holsapple*, 1980; and *Schmidt*, 1980].

Let us assume that an impact with velocity of 20 km s^{-1} is equivalent to an explosion at a scaled depth of burst (SDOB) of ~5 m $kton_{TNT}^{-1/3}$ (1 kton TNT = 4.18×10^{12} Joules). A decrease in impact velocity leads to an increase in the equivalent depth of burst [*Oberbeck*, 1971; *Bryan et al.*, 1980]. The nuclear burst Jungle-U on the SDOB 5 m $kton^{-1/3}$ created in alluvium a crater with the apparent diameter $D_a \simeq 80$ m. Recalculating this value for a rock target and postulating that the volume of a crater in alluvium is twice that of a crater in hard rock (D_a(rock)

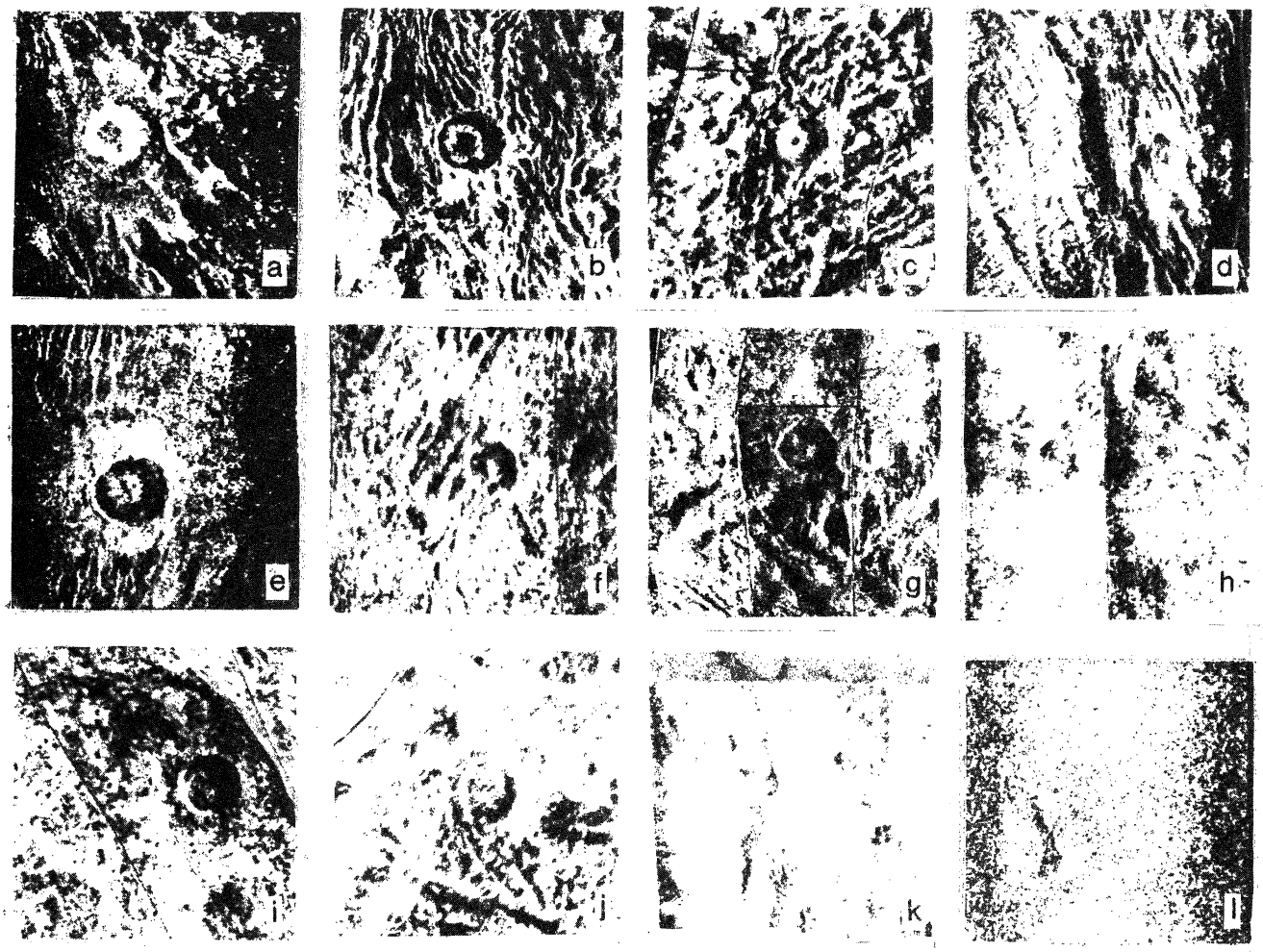

Fig. 8. Craters belonging to various morphological classes, left vertical column-class I, right vertical column class IV. Crater diameters (in km): (*a*) 55, (*b*) 55, (*c*) 35, (*d*) 35, (*e*) 45, (*f*) 35, (*g*) 50, (*h*) 40, (*i*) 35, (*j*) 50, (*k*) 55, (*l*) 35 × 60.

$\simeq D_a$ (alluvium)$/2^{1/3}$ and, assuming that the rim crest diameter is $D_r \simeq 1.25\ D_a$, we derive

$$D_r(m) \simeq 71 \cdot q^{1/3.4}\ (kton) \quad (12)$$

(where q is the explosion yield) for the exponent of scaling according to *Nordyke* [1962]. The transition from explosion yield to impact energy has been done simply by: $q = m_p\ v^2/2$ (m_p is the projectile mass). For crater diameters D_r in kilometers, projectile diameters L_o in kilometers, and impact velocities v in km/s, the last equation can be rewritten as

$$D_r \simeq 2.5\ L_o^{0.882}\ v^{0.588} \quad (13)$$

for a projectile density of $\rho_p = 3000$ kg m^{-3}. If v = 20 km/s then

$$D_r \simeq 16\ L_o^{0.882} \quad (14)$$

The calculations show that the scaling with the kinetic energy of impactors mv^2 rather than the more correct parameter $mv^{0.58}$ for solid targets [*Dienes and Walsh*, 1970] leads to minor errors because of unavoidable violations of the complete scaling laws [*Chabai*, 1977]. However, (14) provides a rather good agreement between numerical impact melt calculations and observed impact melt volumes in terrestrial craters [*Basilevsky et al.*, 1983]. Thus (13) seems to yield lower limits of cratering energy, possibly because of incomplete preservation of impact melts resulting from ejection and erosion.

Another approach developed by *Holsapple* [1980] and *Schmidt* [1980] is based on centrifuge impact experiments with dry sand targets. In this case, two nondimensional parameters

$$\pi_v^* = \rho_t \cdot V/m$$

and (15)

$$\pi_2^* = 3.22\ g \cdot a/v^2$$

TABLE 1. The Relationship Between Maturity and Size of Craters

Diameter range, km	Number of Craters and Percentage (in parentheses) of Total Population Belonging to a Given Class			
	Class I	Class II	Class III	Class IV
8–16	10(40)	10(40)	4(16)	1(4)
16–32	15(23.8)	31(49.2)	13(20.6)	4(6.4)
32–64	8(24)	10(30.3)	12(36.4)	3(9.1)
64–128	1(6.25)	6(37.5)	2(12.5)	7(43.75)

TABLE 2. The Size Distribution of Venusian Craters

	8–11.3	11.3–16	16–22.6	22.6–32	32–45.3	45.3–64	64–90.5	90.5–12.8	128–181
$\Delta N/10^6 km^2$	0.106	0.188	0.318	0.424	0.224	0.165	0.129	0.058	0.024
$\sigma = \sqrt{\Delta N/10^6 km^2}$	0.035	0.047	0.061	0.070	0.051	0.044	0.039	0.026	0.016

σ is standard deviation of the crater density.

are interrelated and may be expressed by

$$\pi_v^* = 0.25\,(\pi_2^*)^{-0.501} \tag{16}$$

where ρ_t is the target density, V is the apparent crater volume, and a is the projectile radius. For $V = D_a^3/36$ (parabolic crater cross-section) and $D_r = 1.25\,D_a$, the D_4 - L_o relation becomes

$$D_r = 2.8\ L_o^{0.833} \cdot V^{0.334} \tag{17}$$

in the units of (13). If v = 20 km s^{-1} then

$$D_r = 8.6\ \cdot L_o^{0.833} \tag{18}$$

for a cylindrical projectile of diameter (l_o) and length (L_o), and a mass equal to a spherical projectile with radius a. Comparing (13) and (14) as well as (14) and (17) indicates that the main difference in the two different approaches arises from the different exponents of velocity. *Ivanov* [1981] has argued that (16) leads to the scaling with the impactor momentum (mv) rather than the value $mv^{0.58}$, especially for solid targets. Therefore the extrapolation of relative low-velocity data for sand, which provide the main argument for (16), seems to possibly overestimate either projectile dimensions and/or velocity. For this reason we have adopted the approach of *Holsapple* [1980] and *Schmidt* [1980] as an upper limit of possible projectile parameters for a given crater. We have used these estimates with (13) and (17) without any correction for an increase of crater diameters by postcratering modifications of the transient bowl-shaped cavity. We feel justified in doing so because our analysis has shown that, for Venusian craters with $D_r \lesssim 100$ km, such corrections would not decrease the estimated value of the projectile diameter versus crater diameter by more than twice. Such corrections would be minor for the most interesting crater diameters, i.e., those near $D_r \simeq 10$ km. The estimated parameters of deformed and decelerated projectiles (see discussion of (10) and (11), substituted in (13) and (17)), illustrate the effect of the Venusian atmosphere on crater dimensions. Figure 14 shows the evaluation for a model target and impactor with a density of 3000 kg m^{-3}. The smallest craters that can be created under the present Venusian atmosphere for low-strength meteoroids are in the range of 7–13 km at zero altitudes and 6–11 km at the altitudes z ≃ 10 km. Unfortunately, these values are very close to the limit of resolution of geological features on the Venera 15/16 images. As a consequence, the paucity of small craters counted on the images may be the result of either atmospheric shielding or marginal image resolution.

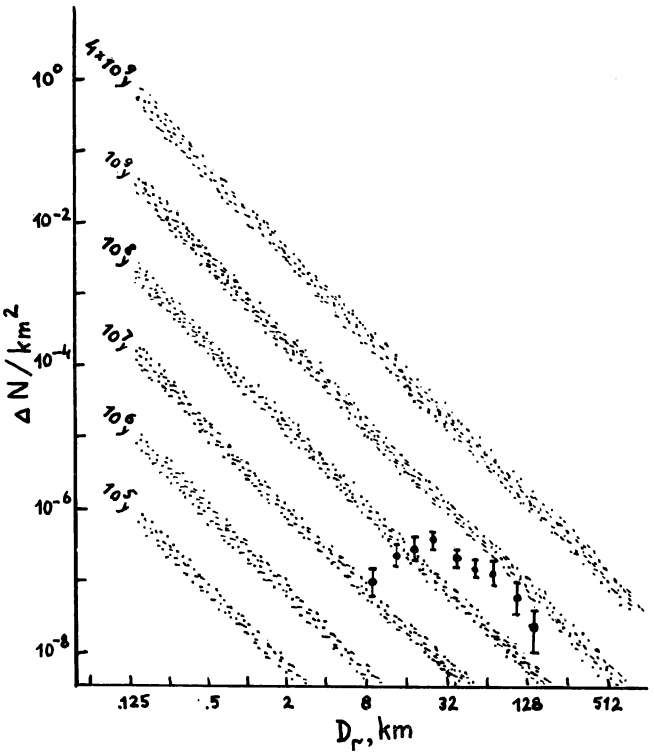

Fig. 9. Veneras 15 and 16 crater densities as a function of crater diameter plotted on Hartmann's diagram [*Hartmann*, 1983].

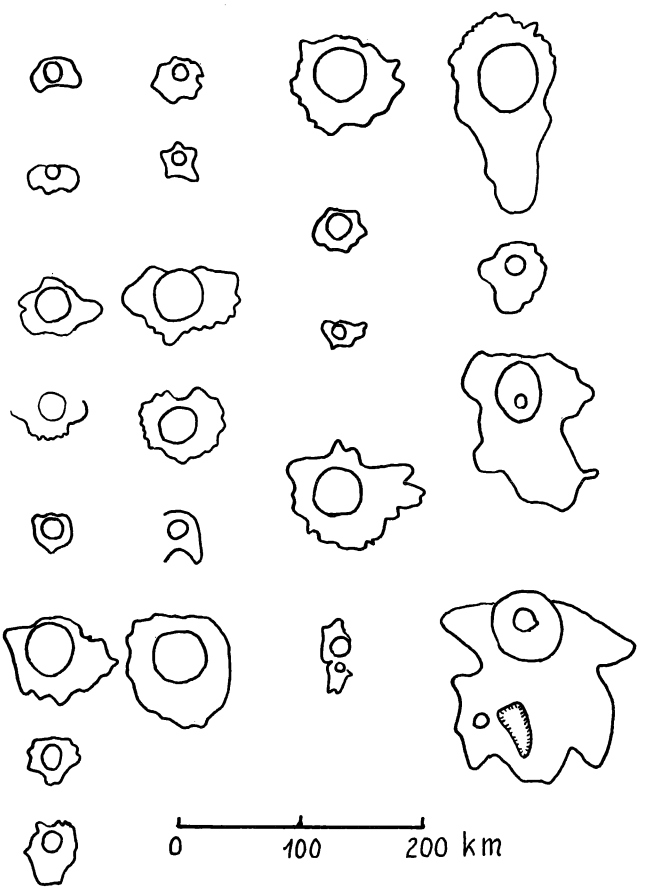

Fig. 10. Shapes of several radar-bright haloes.

TABLE 3. The Maximum Radial Extent from the Center of a Crater of the Radar-bright Haloes (L_m) as a Function of Crater Rim Diameter (D_r)

D_r, km	L_m, km
12	24
12	24
12	24
12	24
12	32
14	38
16	24
16	24
16	32
18	20
20	24
20	40
28	40
32	40
40	52
40	56
40	60
40	72
48	104
52	40
56	112

The average ratio of $L_m/D_r = 1.8 \pm 0.5$.

Our calculations were done for low-strength impactors only. Higher strengths may decrease the deformation of a high velocity projectile at high altitude, but correspondingly high values of the stagnation pressure at low atmospheric altitudes (Figure 12) show that iron bodies would even be deformed inelastically. New calculations are needed, however, for more quantitative conclusions.

The relationships shown on Figure 14 have been used to estimate the degree of distortion of the $\Delta N(D_r) \sim D_r^{-2}$ curve by *Hartmann* [1983], where ΔN is the number of craters per equal logarithmic interval of D_r (usually the log step is $\sqrt{2}$). The estimates assume entry velocity $v = 20$ km/s and a mass distribution consistent with $\Delta N(D_r) \sim D_r^{-2}$ and (10) and (13) for planetary bodies lacking an atmosphere. The distribution of projectile trajectories in space was assumed to be random, so that the number of projectiles entering the atmosphere with angle α to the horizon varied with $\sin \alpha$. The resulting curves in comparison with the observed data are shown in Figure 15. While the use of (10) is more consistent with the observations, the possible underrepresentation of craters near the limit of resolution may lead to an artificial shift of the crater maximum to larger structures.

The general agreement of theoretical and observed crater density curves on Figure 15 shows that the Venusian atmosphere could not have drastically changed through the period of exposure needed to accumulate the observed crater populations. More theoretical calculations as well as new observations are required to determine better constraints on the evolution of the Venusian atmosphere. The first steps of the new work will be to consider impacts by highly deformed, relatively flat projectiles of finite strength, impacting the surface with different trajectory angles.

Finite strength of projectiles would shift the maximum of $\Delta N(D_r)$ curve (Figure 15) higher into the region of smaller D_r. The maximum amplitude of such a shift would be represented by the extreme case of deceleration without any deformation.

3.3. *Shock Waves in the Venusian Atmosphere*

Shock waves are generated by supersonic passage through the atmosphere. These shock waves are similar to those created in the atmosphere with line charge detonators [*Tsikulin*, 1969; *Korobeinikov et al.*, 1973]. The specific energy per unit length of the trajectory (q_e) of a high-velocity body that is transmitted to the atmosphere is expressed as

$$q_e \simeq \pi \rho_a \cdot v^2 \cdot R_o^2 \tag{19}$$

where R_o is the body radius [*Tsikulin*, 1969]. For similar conditions q_e is proportional to atmospheric density. The high density of the Venusian atmosphere leads to high intensity air-shocks that accompany projectile entry.

For instance, a body with velocity $v = 20$ km/s moving in the Venusian atmosphere at zero altitude ($\rho_a = 64.8$ kg m^{-3}) loses energy per 1-km pass length of approximately

$$q_e\ (10^6 \text{ ton of TNT}) \simeq 2500\ R_o^2 \tag{20}$$

where the body radius R_o is expressed in kilometers. This estimate may be rewritten in terms of the body kinetic energy, K

$$q_e \simeq 0.034\ K/R_o \tag{21}$$

(for a body density $\rho_p = 3000$ kg m^{-3}). Hence a body of 1-km radius loses ~3% of its kinetic energy per 1 km of pass length. The lost energy is converted into a high-intensity light and heat flux and to cylindrical shock waves. The radiation heats the gas in front of the bow shock and may drastically affect the gas flow around the body, but it does not strongly influence the estimated air-shock parameters at great distance from the body [*Nemchinov et al.*, 1963, 1976, 1983].

The atmospheric shock waves obey the scaling laws and yield specific relationships of pressure and velocity profiles in time and space, provided that every length value of dimension X is normalized to the characteristic length scale of explosion (W), and every time value by the characteristic time scale of the explosion (τ_w). For a line charge explosion that simulates shock waves generated by a high-velocity body this scales is given by

$$W = q_e^{1/2} \cdot p_a^{-1/2} = \pi \cdot \rho_a/p_a)^{1/2} \cdot v \cdot R_o \tag{22}$$

and

$$\tau_w = W \cdot (p_a/\rho_a)^{1/2} \tag{23}$$

The values of these scalings, estimated for bodies with an initial velocity $v = 20$ km s^{-1} and cratering efficiency according to (10), and normal incidence, $\alpha = 90°$, are given in Table 5. In these estimates the body is treated as undeformed during deceleration by the atmosphere. One can see that the value of linear scales in Table 5 of even small cratering events is comparable with the thickness of the Venusian atmosphere. Therefore all of the following calculations should be treated as qualitative estimates in the model case of a uniform atmosphere.

Figure 16 shows the parameters of a cylindrical shock wave, generated with a line charge of negligible mass in an ideal gas of CO_2 composition with $\gamma = 1.2$ according to numerical calculations by *Kestenboim et al.* [1974]. The scaled rim diameter

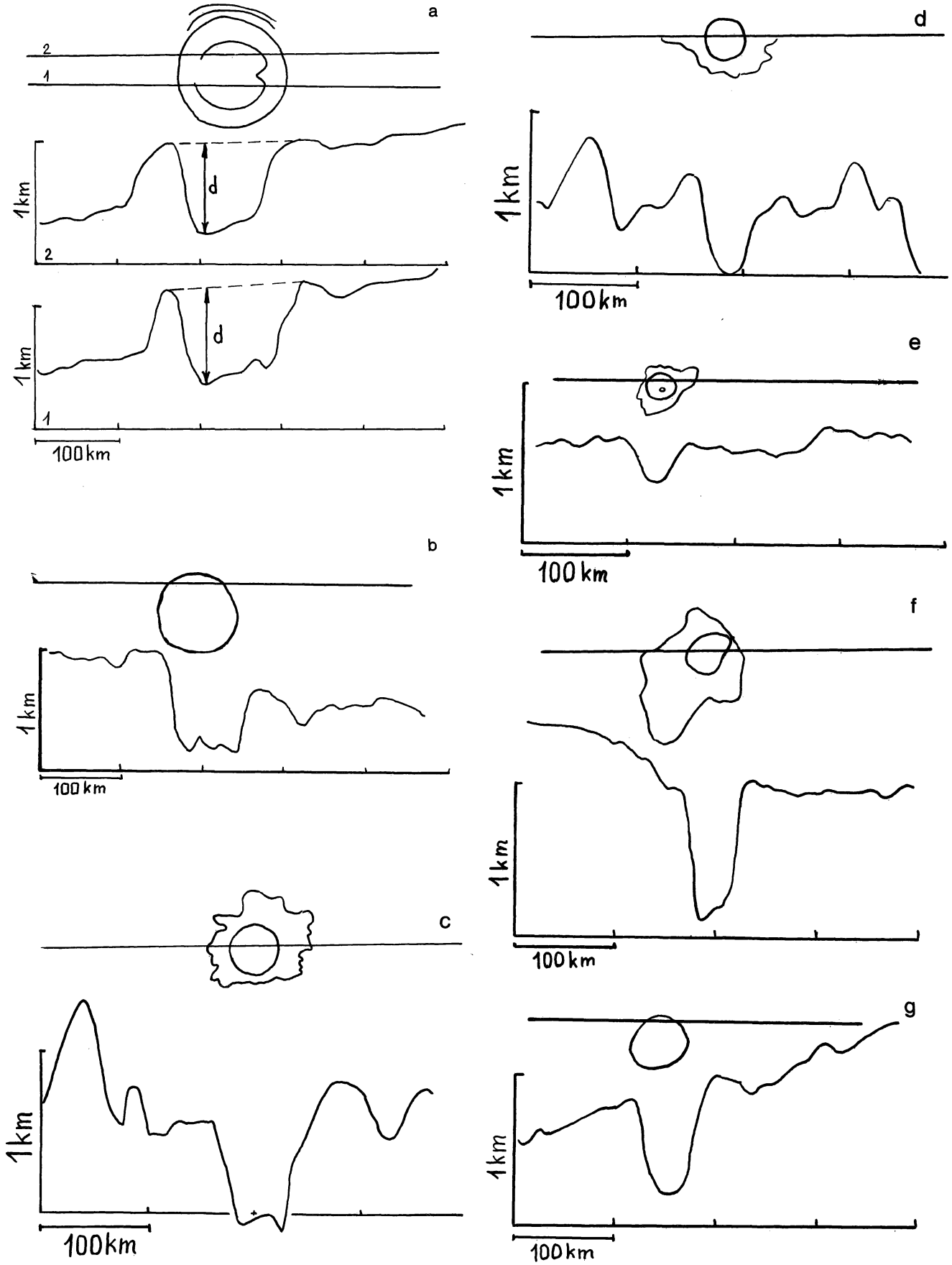

Fig. 11. Depth profiles for several impact craters of Venus. The procedure of crater depth measurements is shown in (*a*).

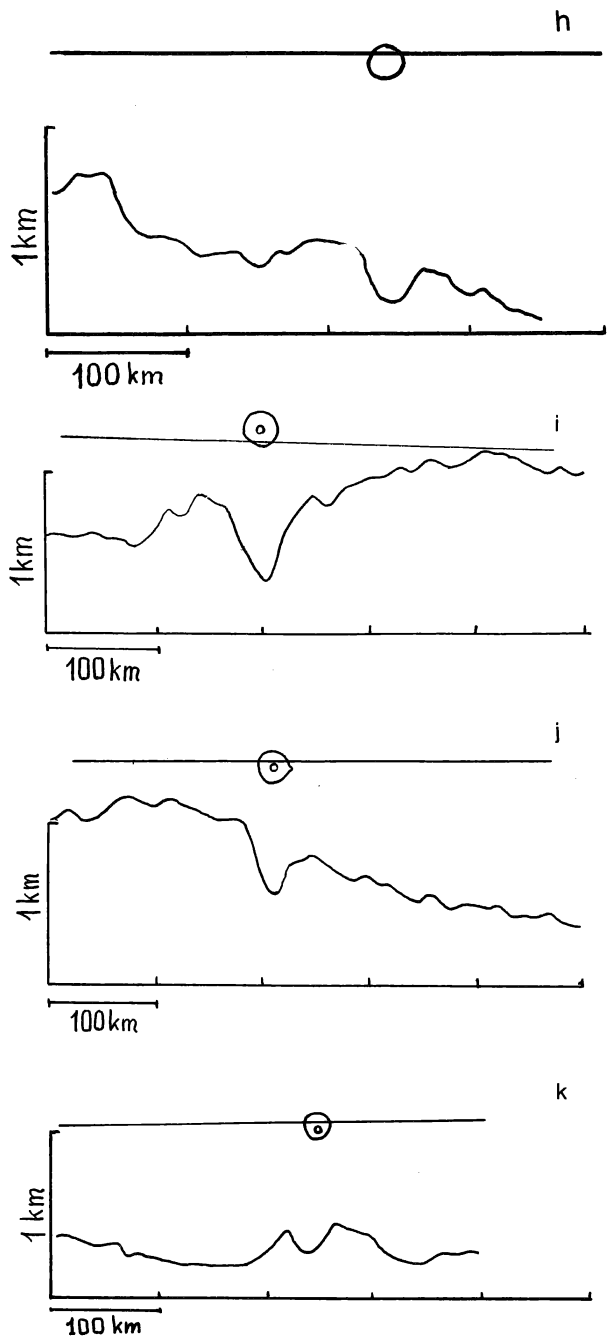

Fig. 11 (continued)

TABLE 4. The Depths of Venusian Craters Obtained from Altimeter Measurements

Crater Diameter, km	Maximum Measured Depth on Profile, km
24	0.2
24 × 28	0.2
28	0.27
28	0.42
32	0.5
40	0.55
40 × 44	0.4
40 × 48	0.9
50	0.8
50 × 60	0.70
100	0.70
100	2.5
140	0.8; 0.8 two profiles

See Figure 11*a* for measurement procedure.

is about $D_z/W \simeq 0.2$. The scaled crater rim radius is about $R_r/W = 0.1$ (cf. Table 5). Some numerical estimations are presented in Table 6.

The most interesting feature is a low residual gas density tube along the trajectory of the high-velocity body. The radius of this tube is relatively large with respect to the crater diameter. The occurrence of this low-density column may lead to the following phenomena.

1. Material ejected into this column up to 2–3 R_r distances from the center of the crater would not be affected by the "normal" undisturbed Venusian atmosphere. This property may result in lunarlike ejecta blankets around Venusian craters. In the case of oblique incidence, the ejecta may be channeled along the projectile trajectory.

2. The ejecta deposition may be disturbed by turbulent uplifting of huge volumes of hot gas because of buoyant forces. Such uplifting may result in the transport of dust into the upper atmosphere.

It is important to note that the tube is not empty, but consists of hot gas of low density, but normal pressure. Therefore the

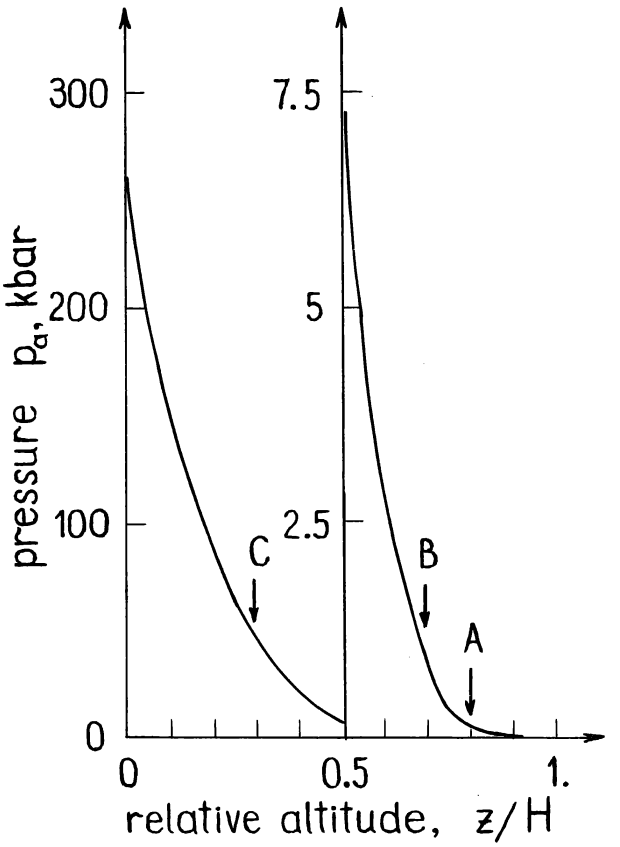

Fig. 12. The maximum pressure (p_a) at the stagnation point of the body moving with a velocity of 20 km s^{-1} as a function of altitude (z) normalized to the effective height of the atmosphere (H, equation (2)). A and B outline the region of the beginning of inelastic deformation of the body. C corresponds to the onset of quasihydrodynamic deformation.

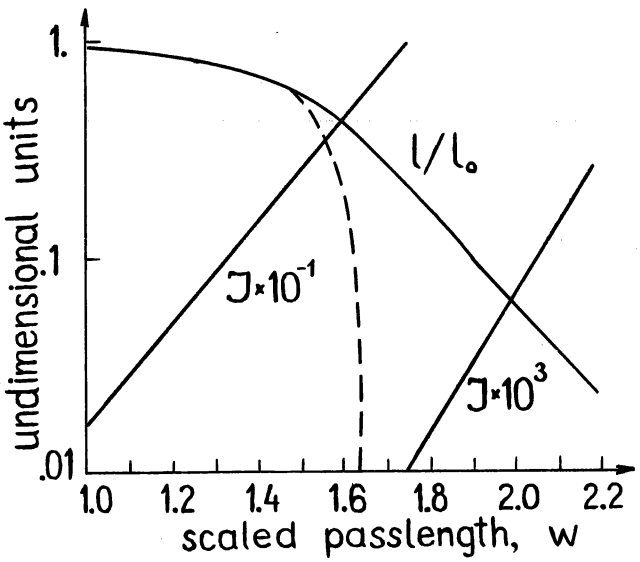

Fig. 13. Decreasing of the projectile thickness, normalized to the initial l/l_0 and to the deceleration function J in equation (11) as a function of scaled distance in the atmosphere w. The impact on the surface of Venus corresponds to $\overline{W}_0 = 2.12(L_0 \sin \alpha)^{-2/7}$ (where L_0 is measured in kilometers and α is the entry angle) for a projectile density 3000 kg m^{-3}. The dashed line corresponds to the model case of a low porosity body (equation (6*a*)).

long-term evolution of this hot tube will not be one of "collapse," but to instead it rises in the ambient, dense atmosphere.

As one can see in Table 6, the air shock may result in direct damage of the ground surface and in a change of its roughness at distances up to 4–6 R_r because:

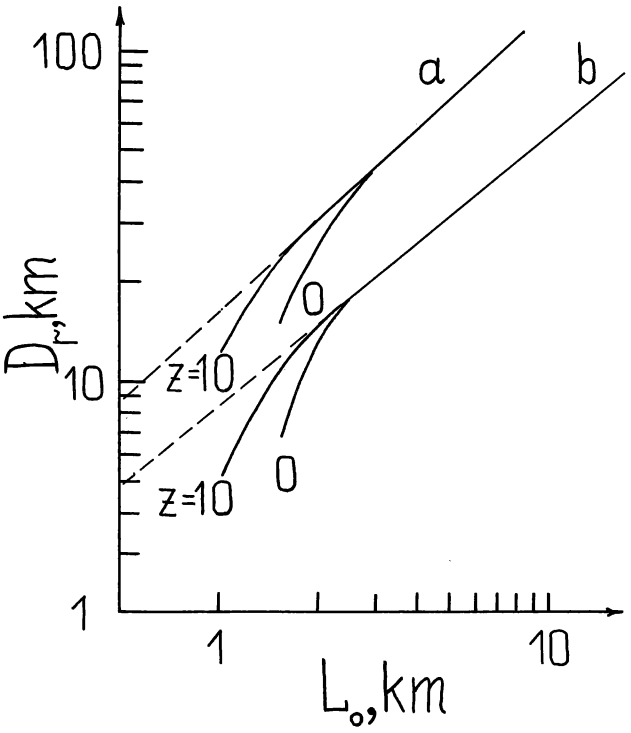

Fig. 14. The calculated crater diameter D_r as a function of the initial projectile dimension L_0(*a*) on the basis of the "explosion" model (equation (10)) and (*b*) on the basis of equation (12). The z values are assumed altitudes in kilometers.

1. The front of a shock wave with a pressure of 100–1000 bar may destroy the surface relief, especially during reflection from obstacles.

2. The dynamic pressure, acting for tens and hundreds of seconds like a very strong wind, may move a large volume of surface material.

3. The negative pressure is not as large as the compressional one but may be able to affect low-strength, porous, and gas-saturated surface rocks. The duration of the negative pressure phase is about $200(D_r/10)$ s (D_r in km).

4. The efficiency of the shock-wave action on the surface may be increased by fragments of the ruptured projectile body, entrained in the air.

5. The geometry of the outer boundary of the zone of the shock-wave action is controlled by the trajectory angle. This effect is well known from the pattern of forest damage caused by the Tunguska 1908 event [see, for example, *Tsikulin*, 1969].

Qualitative estimates of the geometry of dynamic isobars on the surface as a function of the trajectory inclination are shown on Figure 17. The most interesting feature of such patterns is the obvious bilateral symmetry around the trajectory. The radar-bright haloes around craters on Venus may be partially related to the disturbance of the planetary surface around craters by strong air shocks.

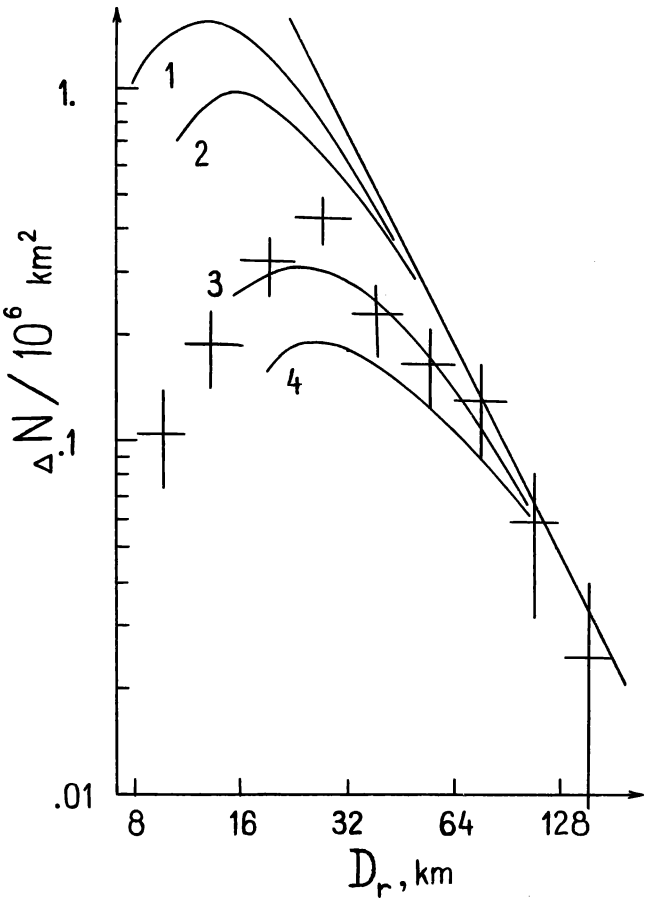

Fig. 15. The observed number Δ N of craters per each log $\sqrt{2}$ increment in diameter intervals per 10^6 km^2 (crosses) in comparison with the model calculation of the atmospheric influence on cratering. Curves 1 and 2 correspond to equation 12 and projectile densities 3000 and 2000 kg m^{-3}, respectively, curves 3 and 4 correspond to equation 10 and the same densities, respectively. Underestimates of small craters may also influence the observed data.

TABLE 5. Approximate Values of Time Scale τ_w and Length Scale W of Atmospheric Cylindrical Shock Wave, Accompanying Venusian Impacts

Crater Diameter D_r, km	Projectile Diameter* L_o, km	Impact Velocity† v, km/s^{-1}	W, km	τ_w/s
10	0.9	12	39	73
20	1.6	15	93	173
40	3.4	17	215	400

*The projectile is assumed to be undeformed.
†Initial velocity is 20 km/s^{-1}.

The ballistic shock wave previously discussed may be followed by shock waves generated as a result of shock vaporization and expansion of these gases.

Our estimates indicate that the interaction of an atmosphere with high-velocity bodies for Venus seems to be included in the dimensional analysis by *Holsapple and Schmidt* [1982].

3.4. The Deposition of the Largest Ejecta Fragments

The problem of a single fragment travelling through the Venusian atmosphere has been numerically calculated for two cases: (1) an undisturbed atmosphere (equation (1)), and (2) an atmosphere disturbed by passage of shock waves.

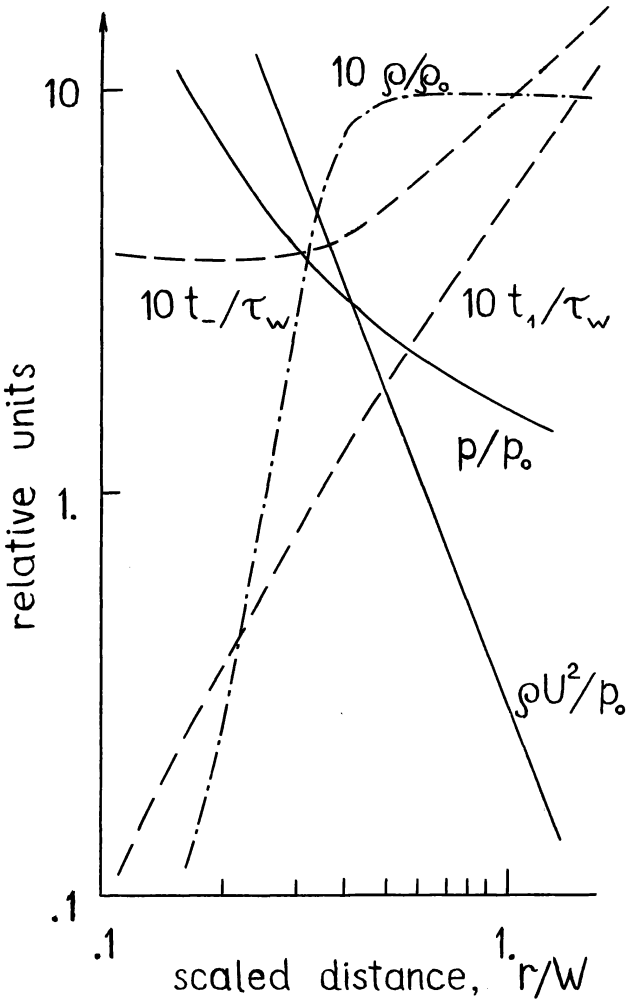

Fig. 16. The scaled dependences of the peak pressure p/p_o, the peak dynamic pressure $\rho V^2/p_o$, the times of the shock front arrival t_1, and of the beginning the negative velocity phase t as well as the residual density profile ρ/ρ_o as functions of scaled distances r/W? in the case of the cylindrical explosion in an ideal gas with $\gamma = 1.2$.

The initial velocity of ejection (v_1) was assumed to be a function of the ejection position r^1

$$v_1 = v_R(r_1/R_a)^{-s_v} \quad (24)$$

where R_a is the apparent crater radius, estimated as $R_a = D_r/2.5$, v_R is a constant with the dimension of velocity, and s_v is an exponent typically $2 < s_v < 3$. The v_R value was derived from the Z-model [*Maxwell*, 1977] according to the Z = 3 case and zero equivalent depth of burst (EDOZ) treated by *Ivanov and Comissarova* [1977] and *Ivanov* [1979]

$$v_R = (4gR_a/15)^{1/2} \quad (25)$$

which describes gravity-dominated cratering and motions.

The ejection angle was assumed constant and equal to $\beta = 45°$ or $\beta = 60°$. The maximum dimension of ejecta fragments for a given crater was described with relationship to the moon [*Ivanov and Basilevsky*, 1982, 1984]

$$d_m(m) = (25 \pm 12)\, D_r^{0.7}\ (\text{km}) \quad (26)$$

This value corresponds to $r_1 = R_a$. The decrease of d_m with decreasing r_1 was modeled with the exponent relationship

$$d_m(r_1) = d_m(R_a) \cdot (r_1/R_a)^{S_d} \quad (27)$$

where S_d is an exponent. The only experimental relationship known to us for the model of underground explosion [*Sizov and Tsvetkov*, 1979] gives $S_d = 2.5$. The value of s_v in (24) was estimated to range from 2.5 to 3 on the basis of laboratory experiments [*Ivanov*, 1977; *Piekutowski*, 1980] as well as numerical calculations [*Cooper*, 1977]. The case of $s_v = s_d = 2.5$ was modeled and is in accordance with *Seebaugh* [1977]. The model of fragmentation was tested with Ries ejecta data [*Hörz et al.*, 1983] with good results.

The ballistic equations were computed with the Runge-Kutt method [see, for example, *Tauber et al.*, 1978]. The time increment was kept small to avoid relative errors of more than 5% in distance. The drag coefficient was assumed according to *Seebaugh* [1977].

For these calculations the ejecta moved initially as a coherent plume, but after a given expansion single body flight becomes appropriate. This plume radius, marking the beginning of single body treatment, was assumed to be

$$r_2 = s_b \cdot r_1 \quad (28)$$

TABLE 6. Gas Dynamic Parameters for a Cylindrical Shock Wave at Specific, Scaled Radial Ranges and at Zero Level of the Venusian Atmosphere (z = 0)

Distance from the Crater Center	R_r	$2R_r$	$4R_r$	$8R_r$
Peak pressure, bar	2,160	675	270	180
Dynamic pressure, bar	13,500	1,800	270	45
Duration of positive phase of dynamic pressure, $\tau_t(D_r/10)$/s	35	31	28	35
Maximum of negative pressure p — p_o/bar	—	−12	−10	−7
Residual density of gas after shock wave passage, kg/m^{-3}	1	1.6	52	63

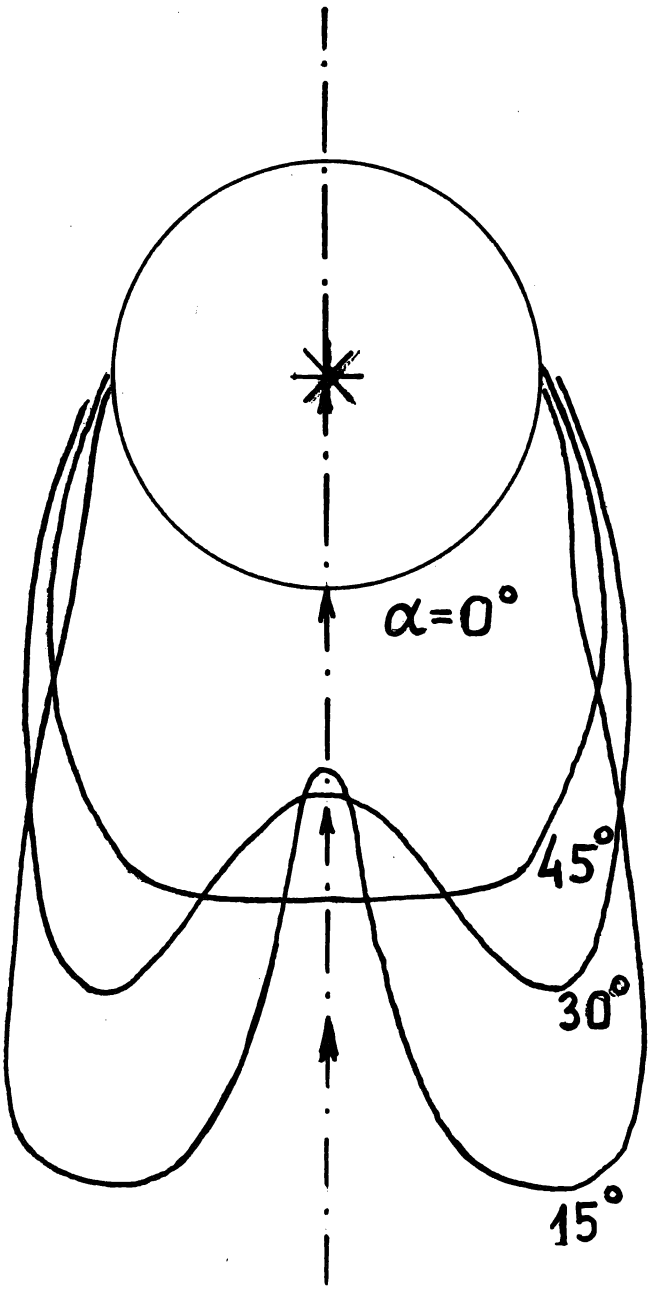

Fig. 17. Qualitative estimates of the geometry of the equal peak dynamic pressure lines for different angle of the trajectory inclination. γ is angle from a horizon.

For a typical value $s_b = 2$, two fragments of equal size moving along radii from the crater center would be separated by a distance equal to their size. The assumed density of individual ejecta fragments was 3000 kg m^{-3}. The ground level altitude was assumed equal to zero and to 10 km. The base set of parameters and its variations are presented in Table 7.

Figure 18 illustrates the results of the calculations. The maximum distance of ejecta emplacement (L_m) for fragments of maximum sizes does not exceed ~$2R_r$ for craters with D_r < 40 km. For larger D_r the relative value of L_m may be larger because of the flight of fragments through the low density upper atmosphere.

TABLE 7. Numerical Parameters Used in the Numerical Ejecta Calculations for the Case of an Undisturbed Atmosphere

	β	S_b	S_v	S_d	Coefficients in (20)
The base case	45°	2.0	2.5	2.5	25
Variations	60°	3.0	3.0	1.0	13
		1.0			37

To estimate the effects of gas movement and heating behind the shock waves, the model problems of simultaneous shock propagation in a uniform atmosphere and moving ejecta were calculated. The scales of the events are given in Table 5. The integration of the ballistic equation has been done with the interpolation of ideal gas data tables by *Kestenboim et al.* [1974]. Only the cases of $10 \leq D_r$ (km) ≤ 40 have been computed, because for more energetic events the density gradient of the atmosphere seemed to be the principal parameter.

The results of the shock-wave model, illustrated in Figure 18, show that the occurrence of a low-density, hot gas zone behind the shock wave allows the transport of ejecta to approximately 1.5 times greater distances than in the case of a static atmosphere. The maximum ejecta distance is practically defined by the size of the low density region only. Thus one may assume that gas dynamic effects that heat the atmosphere during the projectile passage do not drastically restrict the ejecta

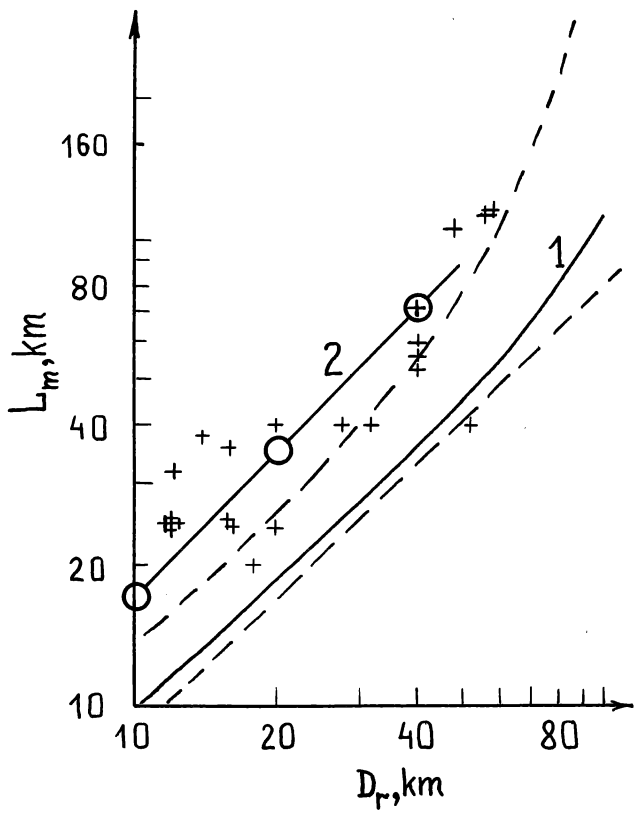

Fig. 18. The calculated maximum radial ranges of ejecta emplacement (L_m) on Venus as a function of crater diameter (D_r). Solid line 1 corresponds to the basic model case of an undisturbed atmosphere; dashed lines mark possible variations depending on the model (see Table 7). Solid line 2 with circles shows the data of the shock-wave model. Crosses are observed values for radar-bright haloes around Venusian craters.

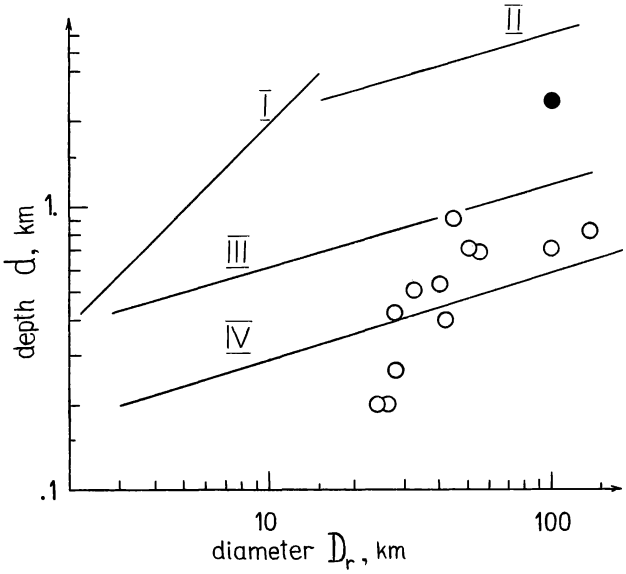

Fig. 19. The depth-diameter data on the Venusian craters, from direct radar altimetry profiles (circles) I and II are the lunar relationships, respectively, for simple and complex craters [*Pike*, 1977], and III is the lunar curve, scaled to the higher Venusian gravity. IV is the relationship to Earth [from *Grieve and Head*, 1982]. The black circle corresponds to Cleopatra Patera.

distribution on Venus. This postulate may be an explanation of the observed rather large depths of the Venusian craters. Estimates of the distance of ejecta show that the ejecta may be responsible for the formation of radar-bright haloes around some of the Venusian craters.

4. DISCUSSION

The study of the morphology and number-versus-diameter statistics of Venusian craters leads to some planetological conclusions, including some constraints on the characteristics of the environment of Venus, in particular its atmosphere.

4.1. Crater Density Statistics

The crater-size distribution for 139 craters on Venus counted on an area of about 85×10^6 km^2 are compared to Hartmann's diagram [*Hartmann*, 1983] in Figure 9. The curve of observational data has a maximum in the 22.6–32 km range. On the whole it is very similar to the model curve (Figure 15) obtained with the assumption of complete destruction of projectiles below some critical size and by deceleration of larger projectiles, accompanied by significant deformation. In this work we developed first order estimates of the effects of a dense atmosphere on the crater density statistics for projectiles of density 2000–3000 kg/m^3 and an atmospheric entry velocity 20 km/s. The theoretical curves constrain the observational data and permit an estimation of an "atmosphereless" crater distribution in the form $\Delta N \sim D^{-2}$, which of course will predict more craters than actually observed. A comparison of the "atmosphereless" situation on Venus with Hartmann's lunar graph [*Hartmann*, 1983] permits estimation of an average age of the surface under study as young as 0.5 to 1.0×10^9 years.

The reasonable agreement between the theoretical and experimental curves of $\Delta N(D_r)$ (Figure 15) permits the conclusion that, during the time of formation of this crater population (0.5 to 1.0×10^9 years), the physical characteristics of the Venusian atmosphere did not change significantly.

4.2. Radar-bright Haloes Around Craters

The radar-bright haloes around fresh craters seem to result from the high degree of surface roughness at the scale of the radar wavelength (8 cm) and larger. Based on the theoretical analyses of crater formation in the Venusian environment (section 3 of this paper), we conclude that formation of the radar-bright haloes is caused by at least two mechanisms: (1) direct impact of the atmospheric shock, which is further enhanced by projectile fragments entrained in the gas; and (2) the effects of crater ejecta on the surrounding terrain is limited by the size and duration of the low-density, hot gas along the trajectories. It was mentioned above that radar-bright haloes have, as a rule, a bilateral symmetry. The maximum radial range of the outer boundary of this halo from the crater center can be expressed in the form $L_m = (1.8 \pm 0.5)D_r$. This radial range is somewhat larger than on the moon, where continuous ejecta extend for about 1.2 D_r. The calculated velocities of ejecta on Venus (section 3), which are not very high due to atmospheric deceleration, appear nevertheless sufficient for the generation of surface roughness on the scale of the radar wavelength.

Surface roughness can be increased also by the interaction of ejecta with the rising "fireball" that generates a giant vortex flow in the atmosphere. The position of the outer boundary of the vortex, where the residual density of atmosphere is about 0.9 ρ_o, corresponds to approximately $2D_r$ from the crater center (Figure 16) for impact velocities of 15 to 20 km/s.

Asymmetry of radar-bright haloes can also result from complex interactions of the atmospheric shock associated with oblique impact (Figure 17). In this case, the distance from the center of impact to the contour lines of equal dynamic pressure behind the reflected wave is increased by a factor of 2 or 3 in the direction of the horizontal projection of the entry path in comparison to vertical impact. Assuming that in the latter case the radius of the radar-bright halo is about 1.5 to $2D_r$, one can determine from Figure 16 the parameters on the shock-wave front: pressure 300 to 700 bar, dynamic pressure ρv^2 = 600 to 2000 bar. Taking into account that dynamic pressures of about 100 bar can transport rock fragments as large as 100 m in diameter, it seems quite possible that such a process will yield some surface roughness. At greater distances the lower wind load can have the opposite effect, i.e., terrain-smoothing; this, in turn, may lead to the formation of radar-dark zones around the radar-bright haloes. Such zones can be seen locally in Venera 15 and 16 images (Figure 2), and they are prominent on the Arecibo radar pictures (J. W. Head, personal communication, 1985).

The absence of radar-bright haloes around morphologically mature craters, and assuming that the halo is indeed reflecting high surface roughness, leads to the conclusion that the rough terrain around craters is being progressively subdued by some exogenic processes, most probably by weathering such as aeolian erosion and aeolian deposition. Radar-bright haloes are typical of about 25% of the observed crater population. If these craters are the youngest members of the population, then their ages should be no more than 25% of the total time of accumulation of the observed population (0.5 to 1.0×10^9 years), and assuming constant impactor flux. Therefore the radar-bright haloes are obliterated on a time scale of about 0.12 to 0.25×10^9 years.

If the radar-bright haloes are due to roughness on decimeter-meter scales, one can conclude that exogenic obliteration of the Venusian surface has a rate of decimeters to meters for 0.12 to 0.25×10^9 years or 0.04–0.8 cm/10^6 years.

4.3. *Depth of Craters*

Direct measurements of impact craters on Venus show significant depths for the morphologically prominent craters (Figure 19). To compare the Venusian data with the lunar craters, the lunar depth/diameter function must be adjusted for the Venusian gravity. According to *Pike* [1977], the depth/diameter function for bowl-shaped lunar craters is

$$d = 0.196 \cdot D_r^{1.01} \tag{29}$$

and for craters of complex morphology ($D_r > 15$ km)

$$d = 1.044 \cdot D_r^{0.301} \tag{30}$$

These functions are shown in Figure 19 and I and II, respectively; the curves of (23) and (24) intersect each other at $D \simeq 11$ km. If one assumes according to *Pike* [1980] and *Basilevsky* [1981] that this intersection diameter is inversely proportional to gravity (g), one can estimate the inflection diameter D for Venus's gravity

$$D_{Venus} = D_{moon} \cdot \frac{g_{moon}}{g_{Venus}} \simeq 11 \cdot \frac{1.62}{8.87} = 2 \text{ km} \tag{31}$$

If we find the point on curve I corresponding to the calculated inflection point for Venus and draw a line from this point parallel to line II, we can develop a prediction function for Venusian craters

$$d \simeq 0.3 \cdot D_r^{0.301} \tag{32}$$

This function (25) is designated as III in Figure 19. Line IV in Figure 19 corresponds to terrestrial craters [*Grieve and Head*, 1982]

$$d = 0.14\, D_r^{0.311} \tag{33}$$

One can see from Figure 17 that craters of Venus are rather deep, especially if we take into account the smoothing of the actual profile by the large spot of the altimeter radar. Some of the measured craters have radar-bright haloes, whereas others do not. Their ages can be estimated (see above) to be less or more than $0.12–0.25 \times 10^9$ years, respectively. This indicates that the Venusian crust is sufficiently rigid to sustain large crater depressions for about 10^8 years. The existence of craters with diameters up to 100–140 km that display no evidence of prominent gravity relaxation seems to indicate that the thickness of a rather rigid lithosphere of Venus is several tens of kilometers, at least in the area investigated.

5. CONCLUSIONS

The radar-images of Venus obtained by Venera 15 and 16 space probes show that there are about 140 craters in an area of about 85×10^6 km^2. They show typical impact morphologies and range from 10–150 km diameter. The average age of the surface under study was estimated, using observational data and theoretical models, to be about 0.5 to 1.0×10^9 years. The size distribution of this crater population together with the theoretical model of destruction of the crater-forming projectiles in the dense Venusian atmosphere yields evidence that there have been no significant changes in the physical parameters of the atmosphere of Venus for the last 0.5 to 1.0×10^9 years. Approximately 25% of the craters have a radar-bright halo, generally with a prominent bilateral symmetry, which is probably the result of the greater surface roughness formed by the ejecta deposition and/or the ballistic air-shock wave, generated by high-velocity projectiles passing through the atmosphere. The time of obliteration of the halo-forming roughness of decimeter to meter scales is estimated as approximately one fourth of the total time of accumulation of the observed crater population, i.e., $0.12–0.25 \times 10^9$ years. The relatively large depth of Venusian impact craters indicates that no significant relaxation of craters up to 100–140 km in diameter occurred for a time period on the order of 10^8 years. This implies, at least in some places, the existence of a lithosphere with a sufficient rigidity corresponding to a thickness of no less than several tens of kilometers.

NOTATION

a	radius of spheric projectile.
d	the depth of a crater.
d_m	the size of ejecta fragment.
D_a	the apparent diameter of a crater.
D_r	the rim diameter of a crater.
J	the function of deceleration of a projectile (see Figure 13 and equation (?))
H	the maximum height of the model Venusian atmosphere.
H_o	the thickness of the Venusian atmosphere, condensed to density 64.8 kg m^{-3}.
H_{eq}	the thickness of the Venusian atmosphere
g	the gravity acceleration.
l	the length of a cylindrical projectile.
l_o	the initial l value.
L	the diameter of a cylindrical projectile.
L_e	the characteristic length of the effectively decelerated body ($L_e = H_{eq}$)
L_o	the initial L value.
L_m	the maximum radial extent of the radar-bright halo from the crater center
m	mass of projectile.
ΔN	number of craters per incremental interval in diameter.
p	pressure.
p_a	maximum pressure at the stagnation point of the body traveling through the atmosphere.
p_o	the normal atmosphere pressure.
q	the equivalent energy of impact (usually measured in TNT weight).
q_e	the energy loss of projectile per unit pathlength.
r_1	the radial position of ejection on the ground zero level.
r_2	the radial position of separation of fragments.
R_a	the apparent crater radius.
R_r	the rim crater radius.
s_b	the coefficient in (28).
s_d	the exponent in (27).
s_v	the exponent in (24).
t	time.
T	temperature.
$\vec{u}$	the relative velocity of internal motion of deformed body
v	the velocity of a projectile.
v_o	the initial v value.
v_R	the parameter in (24) with dimension of velocity.
v_1	the initial velocity of ejecta.
W	the scale of length for the description of atmospheric shock (see (22)).
$\overline{W}$	scaled depth of a body in the atmosphere zero is the high boundary of the atmosphere.

α	the angle of trajectory inclination to the horizontal.
B	the initial angle of inclination of ejecta trajectory to the horizontal.
γ	the ratio of heat capacities for ideal gas.
λ	nondimensional parameter in (8).
σ	the standard error of crater counts.
π^*_v, π^*_2	scaled parameters of cratering (see (12)).
ρ	the density of the atmospheric gas.
ρ_o	the density of the Venusian atmosphere at zero altitude (64.8 kg m^{-3}).
ρ_a	the density of the atmosphere at different altitudes.
ρ_p	the density of projectile.
τ_t	the duration of positive pressure in the atmospheric shock.
τ_w	the time scale for the description of the atmospheric shock (see (23)).

Acknowledgments. We thank Valentina P. Shashkina and Natalia N. Bobina for help in the preparation of the manuscript. Luciano B. Ronca helped the authors in preparing the text. Reviewers D. E. Gault and P. Spudis, as well as editors Graham Ryder and Fred Hörz, provided helpful comments. Thanks are extended to our colleagues in the Institute of Radio-engineering and Electronics, USSR Academy of Sciences, and in the Moscow Institute of Energetics for designing the instrumentation and constructing the images that were used in this study.

REFERENCES

Barsukov, V. L., A. T. Basilevsky, A. A. Pronin, R. O. Kuzmin, V. P. Kryuchkov, O. V. Nikolaeva, I. M. Chernaya, G. A. Burba, N. N. Bobina, V. P. Shashkina, V. A. Kotelnikov, O. N. Rzhiga, G. M. Petrov, Yu. N. Alexandrov, A. I. Sidorenko, V. M. Kovtunenko, R. S. Kremnev, A. F. Bogomolov, M. N. Meshkov, N. V. Zherikhin, Yu. S. Tyuflin, E. L. Akim, M. S. Markov, and A. L. Sukhanov, The first results of geological-geomorphological analysis of the radar images of the surface of Venus obtained by spacecrafts Venera 15 and 16 (in Russian), *Dokl. Akad. Nauk SSSR, 279*, 946–950, 1984.

Barsukov, V. L., A. T. Basilevsky, G. A. Burba, N. N. Bobina, V. P. Kryuchkov, R. O. Kuzmin, O. V. Nikolaeva, A. A. Pronin, L. B. Ronca, I. M. Cherbaya, V. P. Shashkina, A. V. Garanin, E. P. Kushky, M. S. Markov, A. L. Sukhanov, A. I. Sidorenko, A. F. Bogomolov, G. I. Skrypnik, M. Y. Bergman, L. B. Kudrin, I. M. Bokshtein, M. A. Kronrod, P. A. Chochia, Ty. S. Tyuflin, S. A. Kadnichansky, E. L. Akim, The geology and geomorphology of the Venus surface as revealed by the radar images obtained by Venera 15 and 16, *Proc. Lunar Planet. Sci. Conf. 16th,* this volume, 1985.

Basilevsky, A. T., On some peculiarities of structure of impact craters on the planets and satellites in solar system (in Russian), *Dokl. Akad. Nauk SSSR, 258*, 323–325, 1981.

Basilevsky, A. T., B. A. Ivanov, C. P. Florensky, O. I. Yakovlev, V. I. Feldman, and L. B. Granovsky, *The Impact Craters on the Moon and Planets* (in Russian), Moscow, Nauka Press, 200 pp., 1983.

Beliakov, L. V., F. F. Vitman, and N. A. Zlatin, On the processes of impact of deforming bodies and its simulation (in Russian), *Zh. Tekh. Fiz., 34*, 519–592, 1964.

J. B. Bryan, D. E. Burton, L. A. Lettis, L. K. Morris, and W. E. Johnson, Calculations of impact crater size versus meteorite velocity (abstract), in *Lunar and Planetary Science XI*, pp. 112–114, Lunar and Planetary Institute, Houston, 1980.

Chabai, A. J., Influence of gravitational fields and atmospheric pressures on scaling of explosion craters, in *Impact and Explosion Cratering*, edited by D. J. Roddy, R. O. Pepin, and R. B. Merrill, pp. 1191–1214, Pergamon, New York, 1977.

Cooper, H. F., A summary of explosion cratering phenomena relevant to meteor impact events, in *Impact and Explostion Cratering*, edited by D. J. Roddy, R. O. Pepin, and R. B. Merrill, pp. 11–44, Pergamon, New York, 1977.

Dienes, J. K., and J. M. Walsh, Theory of impact: Some general principles and the method of Eulerian codes, in *High-Velocity Impact Phenomena*, edited by R. Kinslow, pp. 45–104, Academic, New York, 1970.

Florensky, C. P., A. T. Basilevsky, N. N. Grebennik, The relationship between lunar crater morphology and crater size, *The Moon, 16*, 59–70, 1976.

Gault, D. E., and J. A. Wedekind, Experimental studies of oblique impact, in *Proc. Lunar Sci. Conf. 9th*, 3843–3875, 1978.

Grigoryan, S. S., On the motion and destruction of meteorites in the planet atmospheres (in Russian), *Kosm. Issled. XVII*, 875–893, 1979.

Grieve, R. A. F., and J. W. Head, The impact cratering process on Venus (abstract), in *Lunar and Planetary Science XIII*, pp. 285–286, Lunar and Planetary Institute, Houston, 1982.

Hartmann, W. K., Relative crater production rates on planets, *Icarus, 31*, 260–276, 1977.

Hartmann, W. K., *Moons and Planets*, Wadsworth, Belmont, 1983.

Holsapple, K. A., The equivalent depth of burst for impact cratering, in *Proc. Lunar Planet. Sci. Conf. 11th*, 2379–2401, 1980.

Hörz, F., R. Ostertag, and D. Rainey, Bunte Breccia of the Ries: Continuous deposits of large impact craters, *J. Geophys. Res., 21*, 1667–1725, 1983.

Ivanov, B. A., The simple model of cratering (in Russian), *Meteoritika, 38*, 68–85, 1979.

Ivanov, B. A., and A. T. Basilevsky, On the fragment-size distribution of ejecta of impact craters (abstract), in *Lunar and Planetary Science XIV*, pp. 345–346, Lunar and Planetary Institute, Houston, 1983.

Ivanov, B. A., and A. T. Basilevsky, Estimations of maximum size of fragments in ejecta from impact craters, in *Abstracts of XVIII Conference on Meteoritics and Cosmochemistry* (in Russian), pp. 115–117, Chernogolovka, 1984.

Ivanov, B. A., and L. I. Comissarova, The simple hydrodynamic model of cratering, in *Lunar Science VIII*, pp. 499–501, The Lunar Science Institute, Houston, 1977.

Keestenboim, Kh. S., G. S. Rosliakov, and L. A. Tchudov, *Point Source Explosion* (in Russian), Nauka, Moscow, 255 pp., 1974.

Knowles, C. P., and H. L. Brode, The theory of cratering phenomena: an overview, in *Impact and Explosion Cratering*, edited by D. J. Roddy, R. O. Pepin, and R. B. Merrill, pp. 869–896, Pergamon, New York, 1977.

Korobeinikov, V. P., P. I. Tchushkin, L. B. Shurshalov, On the hydrodynamic effects during flying and explosion of large meteoritic bodies in the Earth atmosphere (in Russian), *Meteoritika, 32*, 73–89, 1973.

Maxwell, D. E., Simple Z model of cratering, ejection and the overturned flap, in *Impact and Explosion Cratering*, edited by D. J. Roddy, R. O. Pepin, and R. B. Merrill, pp. 1003–1008, Pergamon, New York, 1977.

Moroz, V. I., The atmosphere of Venus, *Space Sci. Rev., 29*, 3–127, 1981.

Nemchinov, I. V., M. A. Tsikulin, An estimation of heat-transfer by radiation for large bodies moving through the atmosphere with high velocity (in Russian), *Geomagn. Aeron., 3*, 635–646, 1963.

Nemchinov, I. V., T. I. Orlova, V. V. Svetscov, and V. V. Shuvalov,On the role of radiation for the motion of meteorites with very high velocities through the atmosphere (in Russian), *Akad. Nauk Dokl. SSSR, 231*, 1084–1087, 1976.

Nemchinov, I. V., and S. P. Popov, Hypersonic flow arund the body in the regime of high intensity radiation heat transfer (in Russian), *Izv. Akad. Nauk SSSR, Mekh. Zhidk. Gaza, 5*, 126–129, 1983.

Nordyke, M. D., An analysis of cratering data from desert alluvium, *J. Geophys. Res., 67*, 1965–1974, 1962.

Oberbeck, V. R., Laboratory simulation of impact cratering with high explosives, *J. Geophys. Res., 76*, 5732–5749, 1971.

Petrov, G. I, and V. P. Stylov, The motion of large bodies in atmospheres of planets (in Russian), *Kosm. Issled. XIII, 4*, 587–594, 1975.

Piekutowski, A. J., Formation of bowl-shaped craters, in *Proc. Lunar Planet. Sci. Conf. 11th*, 2129–2144, 1980.

Pike, R. J., Size-dependence in the shapes of fresh impact craters on the Moon, in *Impact and Explosion Cratering*, edited by D. J. Roddy, R. O. Pepin, and R. B. Merrill, pp. 489–510, Pergamon, New York, 1977.

Pike, R. J., Control of crater morphology by gravity and target type: Mars, Earth, Moon, in *Proc. Lunar Planet. Sci. Conf. 11th*, 2159–2189, 1980.

Romeo, D. J., and J. R. Sterrett, Flow field for sonic jet exhausting counter to a hypersonic mainstream, *AIAA Journal, 3*, 214–217, 1965.

Schmidt, R. M., Meteor Crater: Energy of formation—implications of centrifuge scaling, in *Proc. Lunar Planet. Sci. Conf. 11th*, 2099–2128, 1980.

Seebaugh, W. R., A dynamic crater ejecta model, in *Impact and Explosion Cratering*, edited by D. J. Roddy, R. O. Pepin, and R. B. Merrill, pp. 1043–1056, Pergamon, New York, 1977.

Sizov, I. A., and V. M. Tsvetkov, On the mechanics of fragment formation in the underground explosion (in Russian), *Fiz. Goreniya i Yzryva, 5*, 108–113, 1979.

Solomon, S. C., and S. K. Stephens, Viscous relaxation of impact topography on Venus (abstract), in *Lunar and Planetary Science XIII*, pp. 752–753, Lunar and Planetary Institute, Houston, 1982.

Schultz, P. H., Impact cratering on Venus (abstract), in *International Conference on the Venus Environment*, p. 6, American Research Center, 1981.

Tauber, M. E., D. B. Kirk, D. E. Gault, An analytic study of impact ejecta trajectories in the atmospheres of Venus, Mars and Earth, *Icarus, 33*, 529–536, 1978.

Trulio, J. G., Ejecta formation: Calculated motion from a shallow-buried nuclear burst, and its significance for high velocity impact cratering, in *Impact and Explosion Cratering*, edited by D. J. Roddy, R. O. Pepin, and R. B. Merrill, pp. 919–958, Pergamon, New York, 1977.

Tsikulin, M. A., *Shock Waves Generated by the Motion of Large Meteoritic Bodies through the Atmosphere* (in Russian), Nauka, Moscow, 88 pp., 1969.

Ullrich, G. W., D. J. Roddy, and G. Simmons, Numerical simulations of a 20-ton TNT detonation on the earth and implications concerning the mechanics of central uplift formation, in *Impact and Explosion Cratering*, edited by D. J., Roddy, R. O. Pepin, and R. B. Merrill, pp. 959–982, Pergamon, New York, 1977.

B. A. Ivanov, O. Yu. Schmidt Institute of the Earth Physics, USSR Academy of Science, Moscow.

A. T. Basilevsky, V. P. Kryuchkov, I. M. Chernaya, V. I. Vernadsky Institute of Geochemistry and Anlytical Chemistry, USSR Academy of Science, Moscow.

(Received March 15, 1985;
revised August 6, 1985;
accepted September 18, 1985.)